

Multichannel Impedance Cytometry Downstream of Cell Separation by Deterministic Lateral Displacement to Quantify Macrophage Enrichment in Heterogeneous Samples

Karina Torres-Castro, Javad Jarmoshti, Li Xiao, Aditya Rane, Armita Salahi, Li Jin, Xudong Li, Federica Caselli, Carlos Honrado,* and Nathan S. Swami*

The integration of on-chip biophysical cytometry downstream of microfluidic enrichment for inline monitoring of phenotypic and separation metrics at single-cell sensitivity can allow for active control of separation and its application to versatile sample sets. Integration of impedance cytometry downstream of cell separation by deterministic lateral displacement (DLD) for enrichment of activated macrophages from a heterogeneous sample is presented, without the problems of biased sample loss and sample dilution caused by off-chip analysis. This requires designs to match cell/particle flow rates from DLD separation into the confined single-cell impedance cytometry stage, the balancing of flow resistances across the separation array width to maintain unidirectionality, and the utilization of co-flowing beads as calibrated internal standards for inline assessment of DLD separation and for impedance data normalization. Using a heterogeneous sample with un-activated and activated macrophages, wherein macrophage polarization during activation causes cell size enlargement, on-chip impedance cytometry is used to validate DLD enrichment of the activated subpopulation at the displaced outlet, based on the multiparametric characteristics of cell size distribution and impedance phase metrics. This hybrid platform can monitor the separation of specific subpopulations from cellular samples with wide size distributions, for active operational control and enhanced sample versatility.

cell types to exhibit subpopulations.^[1] Heterogeneity arising from the phenotypic plasticity of immune, cancer and stem cells that serve multiple biological functions,^[2] some with competing functional roles is important to quantify, since their balance regulates emergence of several diseases^[3] and therapeutic outcomes. Hence, specific cellular subpopulations need to be enriched for quantifying their functional role and identifying disease markers.^[4,5] While this is performed effectively by flow cytometry after fluorescent staining^[6] or magnetic functionalization^[7] of characteristic surface proteins, followed by fluorescent or magnetic activated cell sorting, the sample preparation is time consuming, requires costly chemicals, and introduces selection bias. Additionally, these operations are done off-chip, which causes sample loss, dilution and limits the enrichment level possible for fractional subpopulations. Furthermore, characteristic cell surface markers are often not available for biological functions, such as cancer metastasis,^[8] stem cell differentiation lineage,^[9] and immune cell activation.

^[10] Complementary approaches to identify cell phenotypes based on biophysical differences^[11] in size,^[12] shape,^[13] deformability^[14] and electrical properties^[15] are emerging, but multiparametric approaches for high dimensional identification of

1. Introduction

Phenotypic heterogeneity is an essential feature of the organization and functioning of biological systems, causing specific

K. Torres-Castro, J. Jarmoshti, A. Salahi, C. Honrado, N. S. Swami
Department of Electrical Engineering
University of Virginia
Charlottesville, VA 22904, USA
E-mail: carlos.honrado@inl.int; nswami@virginia.edu

L. Xiao, L. Jin, X. Li
Department of Orthopedics
School of Medicine
University of Virginia
Charlottesville, VA 22904, USA

A. Rane, N. S. Swami
Department of Chemistry
University of Virginia
Charlottesville, VA 22904, USA

F. Caselli
Department of Civil Engineering and Computer Science
University of Rome Tor Vergata
00133 Rome, Italy

 The ORCID identification number(s) for the author(s) of this article can be found under <https://doi.org/10.1002/admt.202201463>.

© 2023 The Authors. Advanced Materials Technologies published by Wiley-VCH GmbH. This is an open access article under the terms of the Creative Commons Attribution-NonCommercial-NoDerivs License, which permits use and distribution in any medium, provided the original work is properly cited, the use is non-commercial and no modifications or adaptations are made.

DOI: 10.1002/admt.202201463

cells will be needed to discern subtle differences in subpopulations from the same cell type.^[16] Hence, microfluidic separation based on multiple biophysical criteria integrated with on-chip phenotypic analysis at single-cell sensitivity can enhance discrimination of cellular phenotypes and be applied to enrich for minority subpopulations.^[17,18,19] This phenotypic information is essential for device design, active control of separation conditions,^[20] and sample choice to improve versatility of the workflow^[21,22] and discrimination ability of the separation.

Integration of on-chip cytometry is especially important within passive microfluidic separation systems, such as those based on deterministic lateral displacement (DLD).^[23,24] DLD designs can robustly separate cells at specific cutoff size or deformability levels^[25,26] for sorting microscale cells of close size along displaced versus zigzag streamlines, with a sharp particle size cutoff, minimal clogging, and high throughput.^[27] However, target cell types can exhibit wide size distributions, causing their separation ability to be limited by the relative position of particle size cutoff within the distribution of cell sizes in a heterogeneous sample. On-chip biophysical cytometry for inline monitoring and feedback during DLD can be utilized to screen a particular sample based on its cellular composition and their size distributions, for systematic design of flow resistances and active control of separation force fields^[28,29,30] to advance automation, relax design requirements, and allow application of versatile sample types.

We present the microfluidic integration of multichannel single-cell impedance cytometry^[31,32,33] downstream of DLD separation based on cell size and deformability metrics, so that biophysical quantification of phenotypes for cell size and electrical physiologies can be conducted at multiple outlets on the same chip. The overview layout of the respective sections of this integrated device is in **Figure 1**, including DLD separation

along zigzag versus displaced streamlines based on designed critical size (or D_c) (Figure 1A) per magnified views for the inlets (Figure 1B), the outlets (Figure 1C), and on-chip impedance cytometry (Figure 1D) to measure impedance magnitude ($|Z|$) and impedance phase (ϕZ) over several simultaneously applied frequencies, with off-chip validation of the collected fractions (Figure 1E). Integration of impedance cytometry downstream of inertial separation has been presented,^[10,34] but the flow rate mismatch has motivated modular platforms^[35] or alternate cytometry methods,^[36] that require extensive device footprints. On the other hand, the operating ranges for flow rate and sample throughput of DLD and impedance cytometry have a high degree of overlap, but their integration presents other challenges. While microstructures over a large footprint (cm-scale) and high depth ($>50\ \mu\text{m}$) are required for high throughput DLD separation, on-chip single-cell impedance cytometry at equivalent throughput requires confined geometries for sensitive measurements of the electric field screening by individual cells.^[32,37] This presents challenges associated with microfabrication, balancing of hydrodynamic resistances to match volumetric flows and utilization of co-flowing beads as internal standards for impedance analysis to normalize signals, account for positional dependence and quantify separation metrics, alongside biophysical analysis of cell phenotypes.

To realize the application of DLD separation coupled to impedance cytometry using heterogeneous samples for separation and cytometry of subpopulations on a single chip, we consider size-controlled separation of macrophages to enrich for subpopulations in their activated state. Macrophages are immune effector cells that display a high degree of phenotypic plasticity due to their role in several homeostatic functions.^[38] Their infiltration at injury sites evokes a cascade of activation and associated inflammatory responses,^[39] but disease

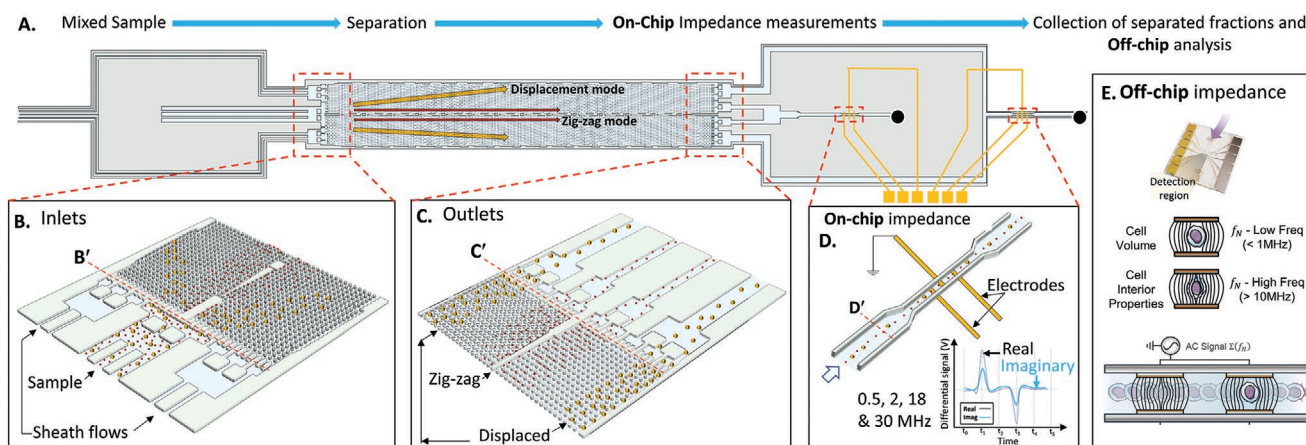


Figure 1. Schematic layout of the different sections of the integrated device: A) Overview of the workflow for DLD in its two separation modes: displacement mode and zig-zag mode. B) Device inlets, wherein mixed samples from the central inlet branches are focused by sheath flows in the lateral inlet branches, and the B' red dashed line shows the input channels for the sheath flows and the sample that feeds each lane of the DLD array. C) Device outlet, wherein the smaller sized sample fraction is collected at the central channel and the larger sized sample fraction is collected at the lateral channels. The C' red dashed line shows the individual outlet DLD array collection channels that are streamlined towards two separate impedance measurement sections, with one for the zig-zag fractions and one for the displaced fractions. D) The two on-chip impedance measurement sections are located after a straight length of channel flow from the DLD outlet region for cytometry of the separated fractions in each outlet and D' red dashed line shows the input channel with a wider volume that decreases towards the impedance section channel. The black filled circles represent the final collection outlets where the two separated fractions are retrieved from the chip. E) The collected samples from the reservoirs of "displaced" and "zig-zag" fractions are analyzed by off-chip impedance cytometry using facing electrodes for validation of on-chip measurements.

outcomes are determined by the balance of activation responses in their subpopulations.^[3] Hence, it is of interest to enrich for subpopulations with activated phenotypes for quantification by cytometry. However, due to their dynamic and stimulus-dependent phenotype,^[40,41] flow cytometry after staining for molecular markers from a specific signaling pathway is often unable to identify the full spectrum of macrophage activation,^[42] or enable longitudinal studies on activation dynamics for the same set of cells within the sample.^[43] Using macrophages (Raw 264.7) stimulated by lipopolysaccharide (LPS) that activates the pro-inflammatory Toll-like receptor 4 (TLR4),^[41] the activation state can be assessed based on impedance magnitude and phase,^[44] which is cross-validated based on the Griess assay for secreted nitrite (NO) in media.^[45] Due to systematic cell size enlargement of macrophages under progressive activation,^[44] akin to that observed during leukocyte activation,^[46] we explore the coupling of DLD-based separation for enrichment of activated macrophages from a heterogeneous sample to on-chip impedance cytometry. This enables multiparametric monitoring of the activation state of the enriched subpopulation, based on the size distribution from impedance magnitude ($|Z|$) and on interior polarization from impedance phase (ϕZ). On-chip quantification of DLD enrichment of the activated macrophage subpopulation from the heterogeneous sample with a distribution of size and activation states prevents many problems observed during sample collection for off-chip cytometry, such as biased sample loss, dilution, and viability loss. Such on-chip integrated approaches to separate and quantify samples

with phenotypic heterogeneity can advance in vitro platforms to screen immunomodulatory drugs for the modulation of macrophage activation.

2. Results and Discussion

2.1. Device Design and Integration

Based on the overview presented in Figure 1, we consider the specific design, integration, and operation tasks. The DLD designs were conducted following standard empirical relations,^[47] with edge corrections to prevent Dean flows in each array period for maintaining unidirectionality, and by shifting the first post in each period to decrease flow disruption when two flows merge. Since unidirectional flow conditions are needed across the device width for ensuring deterministic displacement of particles at the posts, we balanced the hydrodynamic resistance at the inlets before the particles reach the DLD array, for particle separation based on displaced or zig-zag motion at the designed critical diameter (or D_c). Similarly, flow resistances were balanced at the outlet region from DLD, including the additional section leading to the impedance cytometry measurement region, so that the separated fractions can flow into their respective collection channels, without resistance imbalances causing the separated fractions to cross lanes. The CFD simulations in Figure 2A (Supporting Information Section SA3) confirm that the inlet and

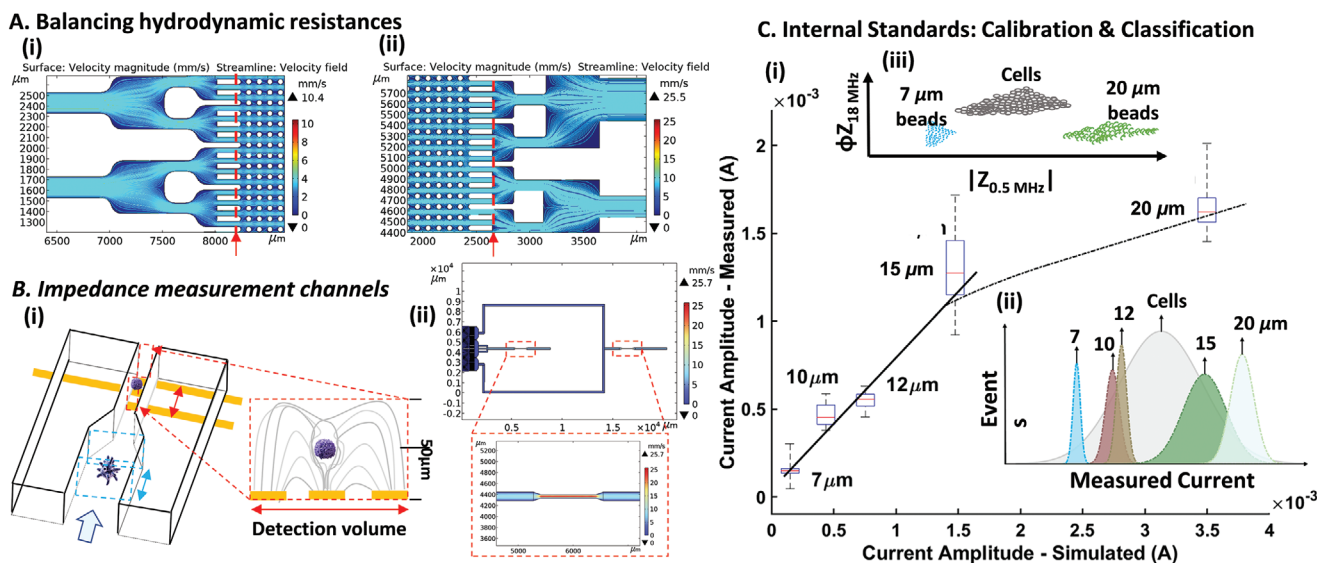


Figure 2. Device design and integration. A) Balancing hydrodynamic resistances across the DLD array inlets and outlets using CFD simulations for design validation (see Supporting Information Section SA3). A(i) shows horizontal flow streamlines at the DLD inlet region. The red dashed line and arrow show the feeding channels for each DLD input lane (B' from Figure 1). A(ii) shows horizontal flow streamlines at the DLD array outlet region that leads to the impedance measurement section. The red dashed line and arrow highlight each DLD array outlet collection lane (C' from Figure 1). B) Impedance measurement in the two outlet channels: The one for the displaced fractions is collected at the edge of the device footprint, and the one for the zig-zag fractions is collected in the device center. B, i) Schematic of impedance measurement channel, with the inset showing the electrodes in the detection volume with respect to a macrophage cell. B, ii) Simulation of DLD device outlet section with two main collection channels, including zoomed in impedance measurement channel showing a significant increase of the flow linear velocity (D' from Figure 1 – also see Figure S5, Supporting Information). C) Co-flowing size-controlled beads as internal standards to assess DLD separation metrics at each outlet and for normalizing the impedance data to enable comparisons across biological sample runs. C, i) Calibration plot to compare measured versus simulated impedance signals using a range of size controlled 7–20 μm beads that spans the range for cells in the sample C(ii), with gating of each population C(iii) (see Supporting Information Section SA4).

outlet branches have a similar level of flow resistance across the device width, thereby ensuring that the flows enter horizontally into the DLD array and split into the required streamlines for effective DLD separation. For coupling the respective DLD separated fractions to impedance cytometry, the volume must be constricted to improve detection sensitivity (Figure 2B(i)), but the data sampling rate must account for the increased flow velocity in the constricted region (Figure 2B(ii); Figure S5, Supporting Information). This was accomplished by constricting the channel volume from the DLD collection region to one-third across a constant 50 μm depth for impedance detection, with a straight section in the impedance channel to stabilize particle flow,^[48,49] prior to detection, using a coplanar electrode design with positional correction.^[50,51] Due to the wide size distribution of cells in heterogeneous biological samples, such as those with subpopulations of activated and un-activated macrophage phenotypes used in this study (8–18 μm), co-flowing size-controlled polystyrene beads must be used in a size range that spans the range for cells in the sample (7–20 μm in Figure 2C(ii)). This will enable their utilization as internal standards to assess separation metrics and to carry out the normalization of impedance cytometry data, by gating each population using a high-frequency ϕZ versus low-frequency $|Z|$ plot (Figure 2C(iii)), to enable comparisons across multiple sample sets. However, the wide size distributions create challenges due to differential focusing of small versus large-sized beads within

the microchannel cross-section and due to amplifier gain settings for the impedance measurements that are optimized for sensitivity to detect smaller beads but may exhibit signal saturation for the larger beads. This was addressed through a calibration plot (Figure 2C(i)), to account for size-dependent focusing using positional correction algorithms based on differential impedance signal shape and for signal saturation by comparing measured versus simulated signal magnitude (details in Supporting Information Section SA4 for signal simulation by COMSOL and for positional correction). Figure 2C(i) confirms proportionality between measured and simulated signal amplitudes in the 7–15 μm range, with a degree of saturation for 20 μm beads, likely due to non-linear gain response of the amplifier. Based on this, we can assess the efficacy of cell separation and carry out impedance signal normalization versus size-controlled beads to account for any temporal variations within the device or sample.

The integrated device set-up (Figure 3A) includes a 3D printed holder to integrate the microfluidic chip for fluidic, electrical, and optical interfacing; the inlet sample and sheathing flows into the DLD array (Figure 3B); and the impedance measurement section downstream from DLD separation, using a custom designed PCB for automated acquisition and triggering of downstream signals (Figure 3C). Also shown are images of flowing mixed sample into the inlet (Figure 3D(i)), the separated fractions after DLD separation into their respective

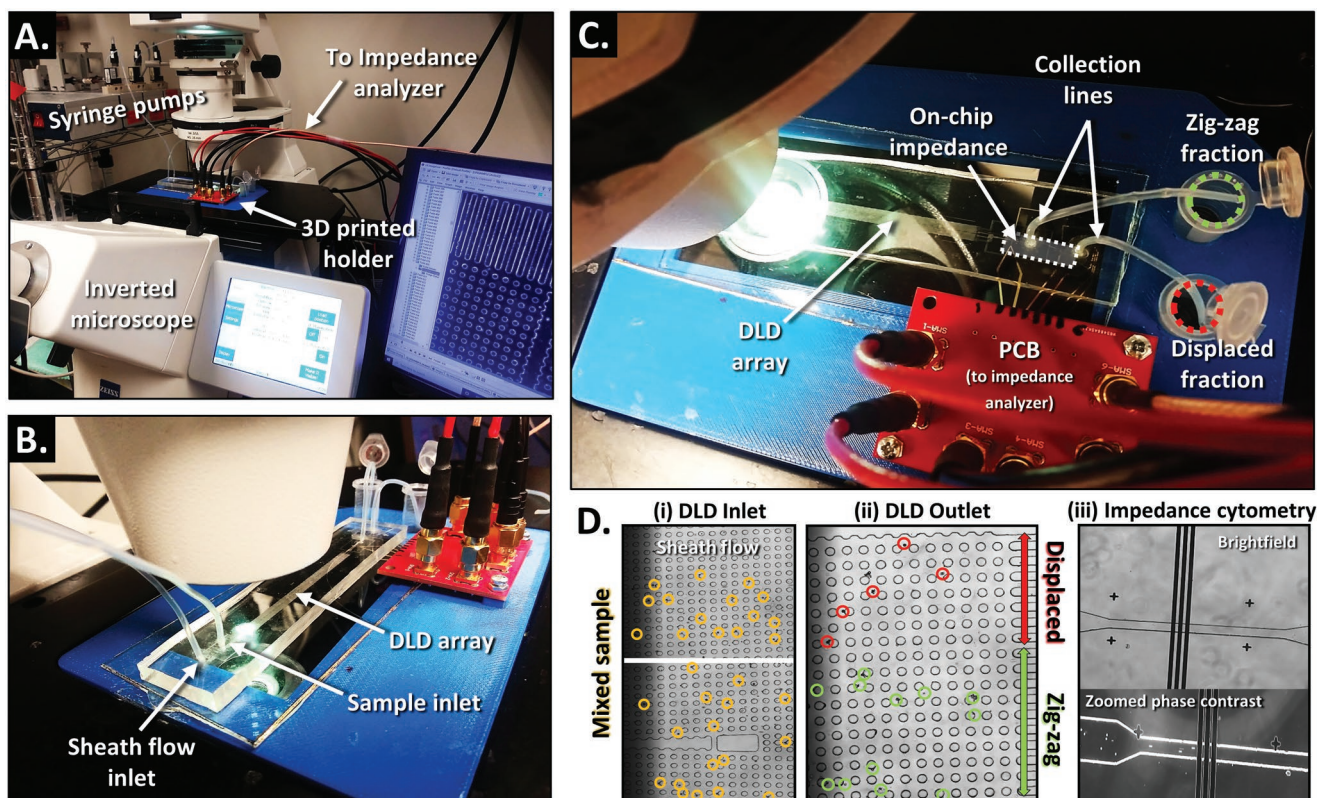


Figure 3. Integrated device. A) 3D printed holder for fluidic, electrical and optical interfacing of the chip for DLD separation and on-chip impedance measurement. B) Close up of the sample and sheathing flows at the inlet. C) Top view of PCB connections to the impedance electrodes, as well as collection of DLD separated fractions. D, i) Images of mixed sample flowing into the inlet, ii) Separated fraction at the end of the DLD array flowing into their respective collection channels and iii) On-chip impedance measurement of displaced cells. (see videos and their description, Section SB1, Supporting Information).

collection channels (Figure 3D(ii)), and the on-chip impedance-based cytometry sections (Figure 3D(iii)).

2.2. Validation of DLD Separation of Beads by On-Chip Cytometry

The integrated device (DLD separation with on-chip impedance cytometry) was assessed for its ability to separate heterogeneous inputs of standard-sized polystyrene beads of differing sizes. Based on images of the fabricated DLD separation array (designed D_C of 11.63 μm becomes fabricated D_C of $12.9 \pm 0.5 \mu\text{m}$, per Figure S4, Supporting Information), we investigated the separation of 7 versus 12 μm (Figure S6A, Supporting Information), 7 versus 15 μm (Figure S6B, Supporting Information), and 7 versus 20 μm beads, using off-chip forward scattering cytometry (FSC) (Figure 4A) and on-chip impedance cytometry (Figure 4B) to measure beads in the input i), zig-zag ii) and displaced outlets iii). Since the actual D_C is likely $\geq 13 \mu\text{m}$, no significant change is observed in the proportion of 7 and 12 μm beads at either outlet for the heterogeneous input sample (Figure S6A, Supporting Information), with very few beads collected in the displaced fraction (<500 events compared to the few thousand events typically measured). However, collection of 15 μm beads predominantly at the displaced

outlet versus a heterogeneous input that includes 7 μm beads (Figure S6B, Supporting Information), confirms that the actual D_C is $< 15 \mu\text{m}$. Using a heterogeneous input of 7 and 20 μm beads, we compare the quantification of separation by off-chip flow cytometry (Figure 4A) versus on-chip impedance cytometry (Figure 4B). While both methods indicate a good level of separation for the smaller-sized beads within the zig-zag outlets and the larger-sized beads within the displaced outlets, on-chip cytometry allows for quantification of the separation with no sample loss at the collection outlets. This is established by confirming that the on-chip detection events of the particles at the respective outlets resemble that of their input proportions using matrix analysis of their cytometry data (Supporting Information Section SB5), but this is not the case for off-chip cytometry of the collected fractions. Weighted mean \pm standard deviations from impedance events confirm sizes of $7 \pm 0.3 \mu\text{m}$ and $20 \pm 0.7 \mu\text{m}$, which are close to vendor standard deviations of 0.2 and 0.3 μm , respectively.

2.3. Application Toward Enrichment of Activated Macrophages

Due to their role within multiple immune functions, the phenotypes of macrophage cells can exhibit a degree of heterogeneity, motivating the need for single-cell measurements. The

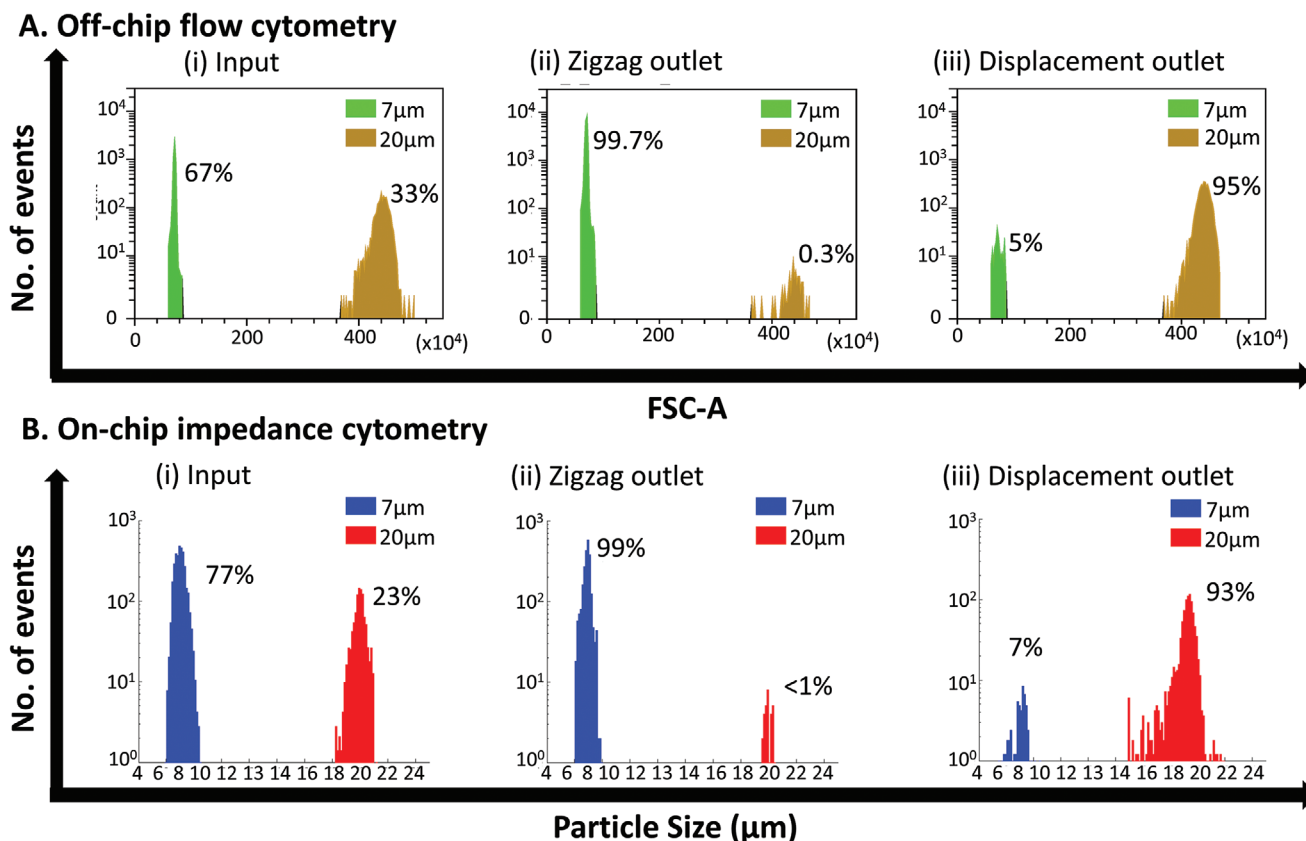


Figure 4. Comparison of: A) off-chip forward scattering flow cytometry (FSC) versus on-chip impedance cytometry ($\sqrt[3]{|Z_{0.5\text{MHz}}|}$) B) for assessing DLD separation of 7 versus 20 μm beads: i) input sample; and fractions in the ii) zig-zag outlet, and iii) displacement outlet. Weighted mean \pm standard deviations from impedance events indicate $7 \pm 0.3 \mu\text{m}$ and $20 \pm 0.7 \mu\text{m}$, which is very close to vendor numbers (See Figure S5, Supporting Information, for trends from flow cytometry for separation of 7 versus 12 μm beads and 7 versus 15 μm beads).

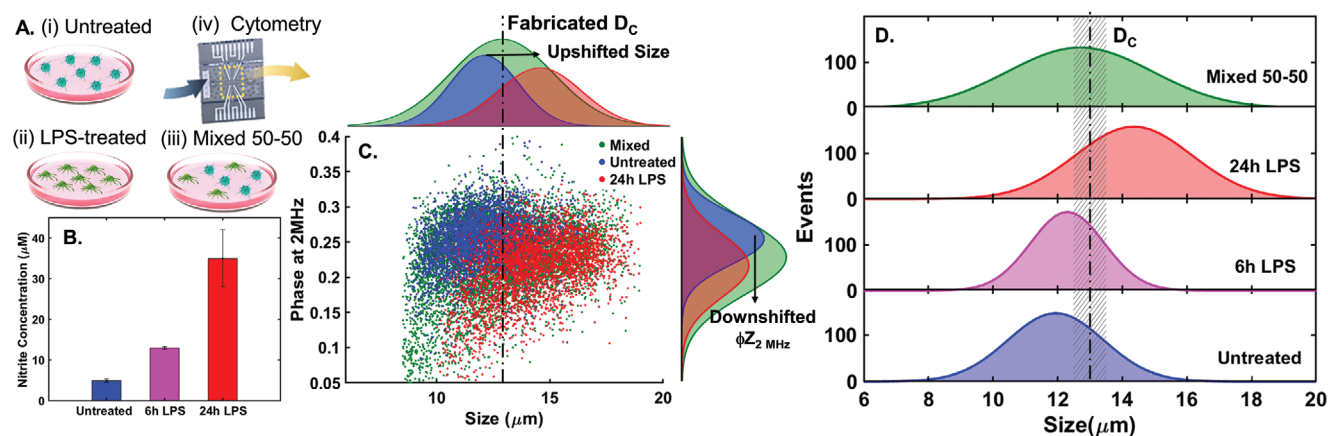


Figure 5. Macrophage activation under LPS-treatment (A(i) versus A(ii)) is validated based on Griess assay for secreted nitrite in media B) and is assessed along with a heterogeneous mixed sample (A(iii)) by single-cell impedance cytometry (A(iv)). C) Activation upshifts the electrical size (or $\sqrt[3]{|Z|_{0.5\text{MHz}}}$) of the cells (x -axis histogram) and downshifts $\phi Z_{2\text{MHz}}$ (y -axis histogram), with the 2D scatter plot showing separation between the data clusters for the untreated and 24 h LPS-treated cells, and with data points in between for the “mixed 50-50 sample” made from equal portions of the above samples. D) The “mixed 50-50 sample” reflects the wide range of sizes observed in the untreated and in the 24 h LPS-treated sample, while its mean size is similar to that of the 6 h LPS-treated sample, suggesting that it is a good representative for a heterogeneous macrophage sample. The fabricated D_C of the DLD array is indicated in (C) and (D), close to intersection point between the size histograms of untreated and 24 h LPS treated samples. Histograms are based on data from ≈ 1000 events for each sample.

heterogeneity can influence their activation state, with the net balance between subpopulations being responsible for the inflammatory response.^[3] Hence, it is of interest to separate and assess macrophage subpopulations based on their activation state to quantify the effect of immunomodulatory drugs on heterogeneity of their activation state. Using $\approx 10^5$ cells per well, stimulation with lipopolysaccharide (LPS) at 100 ng mL^{-1} over a 24 h period causes near-complete macrophage activation (Figure 5A), while LPS activation over a 6 h period activates cells to a lesser extent, as validated by Griess assay for secreted nitrite in the culture media (Figure 5B). However, since the Griess assay averages across all cells in the sample, it cannot assess the heterogeneity in macrophage activation, leading us to consider single-cell impedance cytometry.

Macrophages exhibit systematic increases in cellular electrical size (or $\sqrt[3]{|Z|_{0.5\text{MHz}}}$) with activation,^[44] similar to that observed with leukocyte activation;^[46] hence, we explore the efficacy of DLD-based size separation from a heterogeneous sample to enrich for the activated macrophages in the displaced outlets versus in the zig-zag outlets. Since untreated macrophages are predominantly un-activated and the 24 h LPS-treated samples are predominantly activated, we use a so-called “mixed 50–50” sample, with equal proportions of untreated and 24 h LPS-treated samples to simulate a heterogeneous sample. Impedance cytometry on this mixed sample shows that their cellular electrical size values fall between those of the untreated and 24 h LPS-treated cells (histogram corresponding to the x -axis of impedance scatter plot in Figure 5C). For multiparametric analysis of activated versus un-activated macrophages, we also consider their impedance phase in the MHz range ($\phi Z_{2\text{MHz}}$), which is downshifted upon activation due to their altered interior morphology. The “mixed 50–50” sample shows $\phi Z_{2\text{MHz}}$ levels that fall between those of the untreated and 24 h LPS-treated cells (histogram corresponding to the y -axis of impedance scatter plot in Figure 5C). In fact, while there are some overlaps in the 1D histograms for electrical size and $\phi Z_{2\text{MHz}}$,

the 2D scatter plots of electrical size versus ϕZ (Figure 5C at 2 MHz and Figure S7, Supporting Information, at 0.5 MHz) and the 3D scatter plot (Figure S10, Supporting Information) show a good degree of separation between the data points of the respective parent samples, highlighting the value of multiparametric analysis. The data points for the mixed sample fall in between their parent samples and signals of the two subpopulations (unactivated and activated) can be separated in the 3D plot (Figure S10, Supporting Information). The size distribution of this mixed sample, determined from impedance cytometry, is also compared to its parent sample (untreated and 24 h LPS-treated) in Figure 5D, as well as to the 6 h LPS-treated sample that can exhibit a degree of heterogeneity in impedance phase data due to a mixture of activated and un-activated macrophages (Figure S8, Supporting Information). The average size of macrophages in the mixed 50-50 sample is similar to that of the 6 h LPS-treated sample, but its size distribution reflects the wide range of sizes observed in the untreated and 24 h LPS-treated sample. This suggests that the mixed 50–50 sample is a good representative for a heterogeneous macrophage sample, with a wide size distribution and composed of a mixture of un-activated and activated phenotypes.

The DLD separation was conducted using the mixed 50–50 sample ($\approx 10^5$ cells in 0.5 mL), with on-chip impedance cytometry to monitor the traversing cells in the displaced and zigzag outlets, while the collected fractions at the respective outlets were validated by off-chip impedance cytometry. In comparison to mixed beads that exhibit narrow size distributions of their parent populations, the heterogeneous mixed 50–50 macrophage sample exhibits a wide size distribution in the 8–18 μm range (Figure 5C,D). Hence, while D_C of the DLD array determines the cut-off for size-based separation, the net separation purity depends on the position of D_C with respect to the size distribution histogram of the heterogeneous sample. The small but finite probability for cells slightly smaller than D_C to cross lanes into the displaced outlet and for cells larger

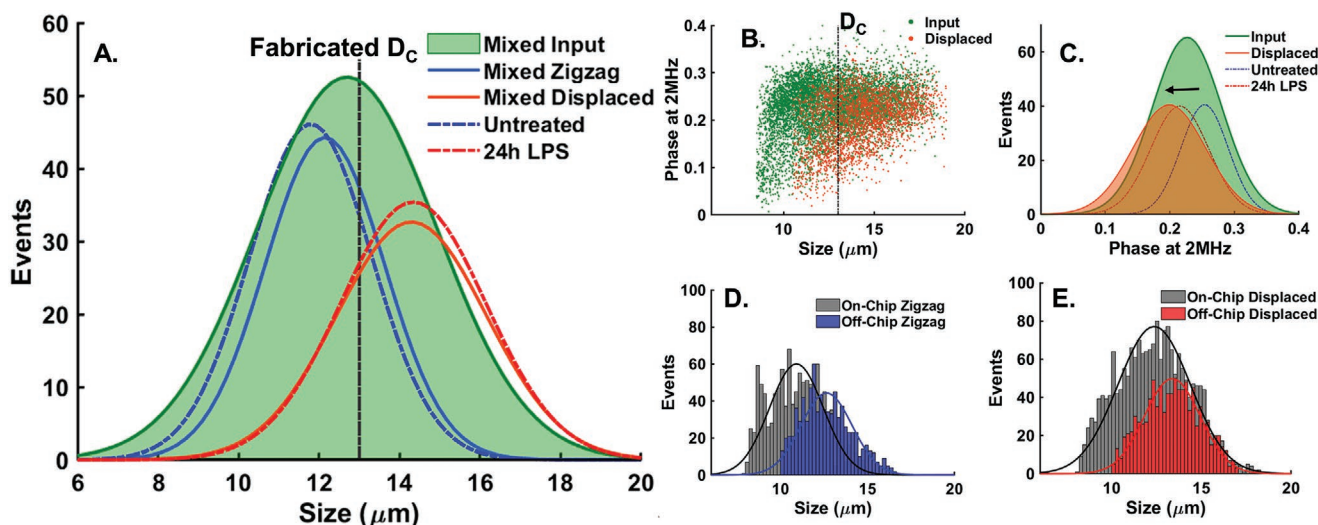


Figure 6. A) DLD separation with on-chip impedance cytometry applied to the mixed 50-50 macrophage sample (equal proportions of untreated and 24 h LPS-treated macrophages) is assessed based on similarity of the size distribution of the displaced fraction to that of the 24 h LPS-treated sample, and that of the zig-zag fraction to the untreated sample. Using an input mixed sample with $\approx 44\%$ of cells $>$ than this D_C value, 72% of cells in the displaced fraction showed cell size levels higher than D_C , which is very close to the expected maximum of the 75% of LPS-treated cells that exhibited sizes $> D_C$. See parallel run in Figure S9, Supporting Information. Cells in the displaced fraction exhibit downshifting of their impedance phase levels (scatter plot in B and histograms of $\phi_{Z_{2\text{ MHz}}}$ in C and $\phi_{Z_{0.5\text{ MHz}}}$ in Figure S6B, Supporting Information), similar to that observed upon activation of macrophages. The size distribution histograms from on-chip impedance cytometry compare well to those from off-chip impedance cytometry for the zig-zag D) and displaced fractions E). All histograms are based on data from ≈ 1000 events for each sample.

than D_C to cross lanes into the zig-zag outlet becomes higher, if the heterogeneous sample contains a large number of cells with sizes near the D_C value for the DLD array. This crossing of lanes can be accentuated at the high flow rates typically used in DLD, since deformation of cells at the posts is more likely for cells of sizes in the vicinity of D_C , thereby causing further deviations in cell streamlines from that determined solely by D_C . The DLD array with a D_C of $\approx 13\ \mu\text{m}$ that is close to the intersection point of the size histograms of untreated and 24 h LPS-treated macrophages and shifted at least one standard deviation away from the mean of the histogram for the mixed 50-50 macrophage sample seems appropriate (Figure 5C). Based on size distributions (Figure 5D), DLD separation based on this D_C would ideally exclude $\approx 80\%$ of untreated sample of unactivated macrophages, and include $\approx 75\%$ of the 24 h LPS-treated sample of fully activated macrophages within the displaced outlet.

On-chip cytometry following DLD separation of the 50-50 sample in Figure 6A shows that the size distribution of the displaced fraction resembles that of the 24 h LPS treated sample that is likely composed of fully activated macrophages and the size distribution of the zig-zag fraction resembles that of the untreated sample that is composed of unactivated macrophages (parallel run in Figure S9, Supporting Information, shows a similar result). Using the input mixed 50-50 sample with $\approx 44\%$ of cells with sizes $>$ than this D_C value, 72% of cells in the displaced fraction after DLD separation showed cell size levels higher than D_C , which is very close to the expected maximum of the 75% of LPS-treated cells that exhibited sizes $> D_C$. The impedance phase levels measured for the cells in the displaced fraction are downshifted with respect to that of the input mixed 50-50 sample (scatter plot in Figure 6B, with histograms of $\phi_{Z_{2\text{ MHz}}}$ in Figure 6C and $\phi_{Z_{0.5\text{ MHz}}}$ in Figure S6B, Supporting

Information), similar to that observed for the 24 h LPS treated activated macrophages versus the untreated macrophages with no activation (Figure 6C). Comparison of the size distributions from impedance cytometry performed on-chip versus off-chip show a good degree of overall similarity (Figure 6D,E), but the histograms suggest that the smaller sized cells picked up by on-chip cytometry are not present within the off-chip cytometry results. Since continued collection of cells is needed over several hours (at least 2 h) to have enough events for off-chip cytometry, it is possible that smaller cells adhere more strongly to the edges of the collection region versus larger cells, thereby causing the reported differences in size data between on-chip and off-chip cytometry. This biased sample loss is similar to that observed with beads (Figure 4) and highlights the need for on-chip cytometry for real-time measurement during DLD separation to improve quantification of enriched sample, as well as ascertain device design (micropost D_C and number of lanes for collection of zig-zag versus displaced fractions), sample (heterogeneity in cell size distributions to account for day-to-day sample variations), and device operational conditions (flow resistance control or electric field based steering) to improve separation within complex samples of unknown heterogeneity.

3. Conclusions

We developed an integrated device with DLD separation coupled to multichannel impedance cytometry for on-chip assessment of phenotypes of the separated fractions from heterogeneous samples that exhibit wide cell size distributions. On-chip cytometry avoids biased sample loss and cross-contamination at the collection outlets, while particle spacing

created by the DLD separation stage reduces coincidence of detection events, thereby preventing dilution of the enriched fractions for off-chip analysis without coincident events. Integration required the ability to maximize cell collection from DLD separation into a confined channel geometry for high sensitivity impedance cytometry, the balancing of flow resistances across the width of the DLD separation array to maintain unidirectional flows, and the utilization of co-flowing beads as calibrated internal standards for assessing DLD separation and for normalization of the impedance cytometry data for effective comparisons across biological samples. Following validation of the DLD separation metrics by on-chip versus off-chip cytometry using a mixed sample of size-controlled beads, the integrated device was applied to enrich for the activated macrophage subpopulation from a model heterogeneous sample with equal proportions of an untreated sample of un-activated macrophages and a 24 h LPS treated sample with activated macrophages. A DLD separation array was designed with a D_C level to ideally include $\approx 75\%$ of the activated macrophages from the 24 h LPS treated sample and exclude $\approx 80\%$ of the un-activated macrophages from the untreated sample within the displaced outlet. This was applied to enrich activated macrophages from the model heterogeneous sample with equal proportions of the untreated and 24 h LPS treated sample. The DLD displaced fraction from this heterogeneous input sample exhibited a size distribution that resembles that of the 24 h LPS treated sample, which is composed of activated macrophages, while the DLD zig-zag fraction exhibited a size distribution that resembles that of the untreated sample, which is composed of un-activated macrophages. Using this input mixed 50-50 sample with $\approx 44\%$ of cells with sizes more than the D_C value, 72% of cells in the displaced fraction after DLD separation showed cell size levels higher than D_C , which is very close to the expected maximum of the 75% of LPS-treated cells that exhibited sizes $> D_C$. Multiparametric analysis based on cell interior characteristics confirmed that the displaced fractions were downshifted in impedance phase levels versus the input sample, further indicating enrichment of activated macrophages at this outlet. The size distributions from on-chip impedance cytometry compare well to that from off-chip cytometry, but biased sample loss was apparent within off-chip cytometry due to the inability to effectively collect the fraction of smaller-sized cells from the device outlet. Future work will focus on the separation of subpopulation from other samples with wide size distributions, such as stem cells and cancer cells, that exhibit size-based phenotypic cutoffs related to stem cell differentiation lineage or cancer metastasis ability.

4. Experimental Section

DLD Device Design and Operation: The DLD device was designed by setting up an array of circular posts with a diameter (D_p) and a gap (G) of 35 μm (fixed parameters). An iterative process, per prior reports,^[23,25] was set up for obtaining a set of critical size (D_C) close to the desired value of $\approx 12 \mu\text{m}$. The selected D_C had a row shift ($\Delta\lambda$) of 3.50 μm . The period or the number of post arrays (N) was iterated such that the total particle displacement ($\mu\text{m}/\text{mm}$) exceeded the post array width in the y -axis (see Supporting Information). The period (N) was adjusted to add redundancy to the DLD device to account for possible

microfabrication defects. The DLD device aspect ratio was kept at 1.43 (50 μm post height). The DLD device was mirrored to increase the cell separation throughput and edge corrections on each array period were done following previously reported empirical relations.^[47] For device operation, two sheath flows were used to confine the input sample in the device center (Figure 1) for maximizing the sample interaction with the DLD post array for enabling the displacement of particles $> D_C$. The volumetric flow proportion between the two sheath flows and the input sample flow was designed to be a 1:1 ratio and the experiment was run by adjusting the flow ratio close to that ratio while keeping the input sample as centered as possible. The overall volumetric flow rate into the device was $\approx 60 \mu\text{L min}^{-1}$.

Microfluidic Device Fabrication and Integration: The device for DLD separation with on-chip impedance measurement was fabricated following the standard photolithography methods. The microfluidic mold was fabricated on a silicon wafer (University Wafer) by spinning SU-8 (2050, Kayaku), soft-baking of the resist, and UV exposure under a photomask on a mask aligner (EVG 620, EV Group, Austria). A post exposure bake was done for evaporating the remaining photoresist solvent and for structural stability. The device structures were examined after the development step and a final hard bake step was done to reduce surface imperfections and enhance mechanical resistance. The electrodes for impedance cytometry were patterned on a glass wafer (University Wafer) using the lift-off technique, by patterning the AZ1505 resist (MicroChemicals GmbH), electron beam deposition (Denton Vacuum) of metals (100 \AA Ti adhesion layer and 1000 \AA Au layer). The metal patterned glass wafer was laser cut (VSL 3.5, Universal Laser Systems, Scottsdale, AZ). The DLD devices were then fabricated using 1:5 of PDMS curing agent to base (Sylgard 184, Dow Chemicals) for soft micromolding. The PDMS was poured into the SU-8 mold on Si, left overnight at 65 $^\circ\text{C}$ on a bake plate (CEE, Apogee), and the PDMS layer was peeled from the mold. Following size estimation of the active PDMS region, and inlets and outlets were drilled using a biopsy punch. The PDMS and glass chip with electrodes were activated using Oxygen plasma (Tergeo, PIE Scientific), aligned to place electrodes in each channel outlet using a stereo microscope, and put in contact for bonding.

Flow Cytometry of Reference Beads: The stock solutions for each bead size (7, 12, 15, and 20 μm from Sigma-Aldrich) were diluted in 1 mL tubes (Flex-tubes, Eppendorf) with 1 \times PBS (Dulbecco, Sigma-Aldrich) and run through the flow cytometer (Cytoflex, Beckman Coulter) for establishing stock solution concentrations. Once those concentrations were known, the volume needed for obtaining an $\approx 50\text{--}50\%$ mix of 7 μm with each of the other bead types (12, 15, or 20 μm) was used to prepare mixed samples and run through the flow cytometer to establish the input sample percentages. Adjustments to the concentration of each bead subpopulation were made to arrive at an approximate 50-50% ratio between beads of each size. Before the DLD separation, the mixed input samples, as well as the collected fractions from the zig-zag and displacement outlets after DLD were run through the flow cytometer for off-chip validation of the separation.

Biological Sample Preparation: Macrophages Raw 264.7 cells from American Type Culture Collection (ATCC) (Manassas, VA) were cultured with Dulbecco's modified Eagle's medium (DMEM, high glucose 4.5 g L^{-1} , Gibco, Grand Island, NY) supplied with 10% fetal bovine serum (FBS) (Gibco), 1% penicillin (100 $\mu\text{g mL}^{-1}$), and 1% streptomycin (100 $\mu\text{g mL}^{-1}$) (Gibco) and maintained in 5% CO_2 at 37 $^\circ\text{C}$. The cell seeding density was optimized to 5 $\times 10^5$ cells mL^{-1} , with 0.5 mL per well, to yield 2 $\times 10^5$ lifted cells per well. For LPS activation, Raw 264.7 cells were pre-seeded in the complete growth media in a 24-well plate at a density of 1 $\times 10^5$ cells mL^{-1} (0.5 mL well) overnight. Cells treated with serum-free media were placed in absence (untreated) or presence of LPS at 100 ng mL^{-1} for 6 and 24 h. Cell secretion analysis for nitrite in culture media was conducted with the Griess assay (Promega, Madison, WI). The heterogeneous sample was made by mixing equal volume portions of untreated and 24 h LPS treated macrophages.

Impedance Cytometry: On-chip impedance cytometry (Figure 1B) was conducted in each outlet channel of the microfluidic device (detection

region $\approx 50 \mu\text{m}$ depth by $\approx 50 \mu\text{m}$ width) at a flow rate of $60 \mu\text{L min}^{-1}$ (neMESYS, Cetoni) in $1\times$ PBS media for the beads and in serum-free culture media for the macrophages to maintain cell viability. AC signals at three discrete frequencies (0.5, 2, and 18 MHz; $2 V_{\text{pp}}$ at each frequency) were applied to the central electrode of the coplanar three-electrode assembly using an impedance spectroscope (HF2IS, Zurich Instruments) and current signal at the adjoining side electrodes was acquired (sample-rate = 1.15×10^{-5} samples s^{-1}) and converted using a current amplifier (HF2TA, Zurich Instruments). Lock-in amplification (HF2TA, Zurich Instruments) was used to separate the real and imaginary signal components at each frequency to compute impedance magnitude and phase (Supporting Information Section SA.1). For off-chip cytometry, samples in each outlet of the DLD device were collected and transferred to a standard chip with facing top-bottom electrodes^[8] (detection region of $50 \mu\text{m} \times 50 \mu\text{m}$) at a flow rate of $\approx 20 \mu\text{L min}^{-1}$, using an impedance analyzer (Ampha Z32, Amphasys AG) at 0.5, 2, 18 and 30 MHz. Processed signal data were then stored in the form of impedance magnitude and phase.

Data Analysis: Impedance cytometry data were processed and analyzed using custom code written in MATLAB (R2018b, MathWorks). The impedance signal was normalized against the frequency-independent impedance response of the reference polystyrene beads by dividing the impedance data by the mean impedance data of reference beads. Due to normalization, impedance phase was herein reported in arbitrary units. Normalized impedance magnitude was used to compute the metric of electrical diameter by calculating $\sqrt[3]{|Z|_{0.5\text{MHz}}}$, and using the polystyrene beads for size reference. Statistical analyses (MATLAB R2018b) were performed on processed datasets. Significance level was defined at $\alpha < 0.05$ for all cases. For cell measurements, two sample Students' *t*-tests were performed to compare individual datasets, to assess statistically significant differences between treatment conditions.

Supporting Information

Supporting Information is available from the Wiley Online Library or from the author.

Acknowledgements

This research was supported by AFOSR grant FA2386-21-1-4070, NSF Award #2051652, DoD PRMRP Discovery Award #192560; University of Virginia's Strategic Investment Fund to establish the Engineering in Medicine Program, the Launchpad Award from the Paul Manning Foundation, and the University of Virginia's Cancer Center through the NCI Cancer Center Support Grant P30 CA44579. The authors thank XuHai Huang of Swami lab and Grace Oh of Li lab for assistance on the samples.

Conflict of Interest

The authors declare no conflict of interest.

Author Contributions

K.T.-C. and J.J. contributed equally to this work. K.T.-C. contributed to conceptualization, investigation, and formal analysis. J.J. contributed to investigation, software, and formal analysis. L.X., A.R., and A.S. performed investigations. L.J. and X.L. contributed to supervision and funding acquisition. F.C. contributed to formal analysis and supervision. C.H. contributed to conceptualization, formal analysis, and supervision. N.S.S. contributed to conceptualization, project administration, supervision, manuscript drafts, resources, and funding acquisition.

Data Availability Statement

The data that support the findings of this study are available in the supplementary material of this article.

Keywords

biophysical cytometry, cell separation, macrophages, microfluidic detection

Received: September 5, 2022

Revised: November 25, 2022

Published online:

- [1] T. J. Perkins, P. S. Swain, *Mol. Syst. Biol.* **2009**, *5*, 326.
- [2] R. Satija, A. K. Shalek, *Trends Immunol.* **2014**, *35*, 219.
- [3] L. Jin, L. Xiao, M. Ding, A. Pan, G. Balian, S.-S. J. Sung, X. J. Li, *Spine J.* **2022**, *22*, 677.
- [4] K. Klepárník, F. Foret, *Anal. Chim. Acta* **2013**, *800*, 12.
- [5] J. Cros, J. Raffenne, A. Couvelard, N. Poté, *Pathobiology* **2018**, *85*, 64.
- [6] D. Włodkowiec, J. Skommer, Z. Darzynkiewicz, *Cytometry, Part A* **2010**, *77*, 591.
- [7] A. Grützkau, A. Radbruch, *Cytometry, Part A* **2010**, *77*, 643.
- [8] J. McGrath, C. Honrado, J. Moore, S. Adair, W. Varhue, A. Salahi, V. Farmehini, B. Goudreau, S. Nagdas, E. Blais, T. W. Bauer, N. S. Swami, *Anal. Chim. Acta* **2020**, *1101*, 90.
- [9] A. R. Yale, J. L. Nourse, K. R. Lee, S. N. Ahmed, J. Arulmoli, A. Y. Jiang, L. P. McDonnell, G. A. Botten, A. P. Lee, E. S. Monuki, *Stem Cell Rep.* **2018**, *11*, 869.
- [10] C. Petchakup, H. M. Tay, K. H. H. Li, H. W. Hou, *Lab Chip* **2019**, *19*, 1736.
- [11] J. Zhou, P. Mukherjee, H. Gao, Q. Luan, I. Papautsky, *APL Bioeng.* **2019**, *3*, 041504.
- [12] Q. Luan, C. Macaraniag, J. Zhou, I. Papautsky, *Biomicrofluidics* **2020**, *14*, 031502.
- [13] C. Honrado, S. J. Adair, J. H. Moore, A. Salahi, T. W. Bauer, N. S. Swami, *Adv. Biol.* **2021**, *5*, 2100438.
- [14] W. B. Varhue, L. Langman, M. Kelly-Goss, M. Lataillade, K. L. Brayman, S. Peirce-Cottler, N. S. Swami, *Lab Chip* **2017**, *17*, 3682.
- [15] A. Rohani, J. H. Moore, Y.-H. Su, V. Stagnaro, C. Warren, N. S. Swami, *Sens. Actuators, B* **2018**, *276*, 472.
- [16] K. C. Lee, J. Guck, K. Goda, K. K. Tsia, *Trends Biotechnol.* **2021**, *13*, 1249.
- [17] S. Yan, J. Zhang, D. Yuan, W. Li, *Electrophoresis* **2017**, *38*, 238.
- [18] N. M. Karabacak, P. S. Spuhler, F. Fachin, E. J. Lim, V. Pai, E. Ozkumur, J. M. Martel, N. Kojic, K. Smith, P.-i. Chen, *Nat. Protoc.* **2014**, *9*, 694.
- [19] F. Fachin, P. Spuhler, J. M. Martel-Foley, J. F. Edd, T. A. Barber, J. Walsh, M. Karabacak, V. Pai, M. Yu, K. Smith, *Sci. Rep.* **2017**, *7*, 1.
- [20] V. Farmehini, S. Kiendzior, J. P. Landers, N. S. Swami, *ACS Sens.* **2021**, *6*, 3765.
- [21] X. Huang, K. Torres-Castro, W. Varhue, A. Rane, A. Rasin, N. S. Swami, *Electrophoresis* **2022**, *43* (12), 1275.
- [22] K. Torres-Castro, C. Honrado, W. B. Varhue, V. Farmehini, N. S. Swami, *Anal. Bioanal. Chem.* **2020**, *412*, 3847.
- [23] A. Hochstetter, R. Vernekar, R. H. Austin, H. Becker, J. P. Beech, D. A. Fedosov, G. Gompfer, S.-C. Kim, J. T. Smith, G. Stolovitzky, *ACS Nano* **2020**, *14*, 10784.
- [24] L. R. Huang, E. C. Cox, R. H. Austin, J. C. Sturm, *Science* **2004**, *304*, 987.
- [25] J. McGrath, M. Jimenez, H. Bridle, *Lab Chip* **2014**, *14*, 4139.

- [26] M. Xavier, S. H. Holm, J. P. Beech, D. Spencer, J. O. Tegenfeldt, R. O. Oreffo, H. Morgan, *Lab Chip* **2019**, *19*, 513.
- [27] K. J. Morton, K. Loutharback, D. W. Inglis, O. K. Tsui, J. C. Sturm, S. Y. Chou, R. H. Austin, *Lab Chip* **2008**, *8*, 1448.
- [28] V. Calero, P. Garcia-Sanchez, C. Honrado, A. Ramos, H. Morgan, *Lab Chip* **2019**, *19*, 1386.
- [29] K. Tatsumi, K. Kawano, H. Shintani, K. Nakabe, *Anal. Chem.* **2019**, *91*, 6462.
- [30] J. P. Beech, K. Keim, B. D. Ho, C. Guiducci, J. O. Tegenfeldt, *Adv. Mater. Technol.* **2019**, *4*, 1900339.
- [31] K. C. Cheung, M. Di Berardino, G. Schade-Kampmann, M. Hebeisen, A. Pierzchalski, J. Bocsi, A. Mittag, A. Tárnok, *Cytometry, Part A* **2010**, *77*, 648.
- [32] T. Sun, H. Morgan, *Microfluid. Nanofluid.* **2010**, *8*, 423.
- [33] C. Honrado, P. Bisegna, N. S. Swami, F. Caselli, *Lab Chip* **2021**, *21*, 22.
- [34] C. Raillon, J. Che, S. Thill, M. Duchamp, B. X. Desbiolles, A. Millet, E. Sollier, P. Renaud, *Cytometry, Part A* **2019**, *95*, 1085.
- [35] T. N. Pahattuge, I. M. Freed, M. L. Hupert, S. Vaidyanathan, K. Childers, M. A. Witek, K. Weerakoon-Ratnayake, D. Park, A. Kasi, M. F. Al-Kasspoles, *ACS Sens.* **2021**, *6*, 1831.
- [36] J. Che, V. Yu, E. B. Garon, J. W. Goldman, D. Di Carlo, *Lab Chip* **2017**, *17*, 1452.
- [37] J. Zhong, P. Li, M. Liang, Y. Ai, *Adv. Mater. Technol.* **2022**, *7*, 2100906.
- [38] D. M. Mosser, J. P. Edwards, *Nat. Rev. Immunol.* **2008**, *8*, 958.
- [39] S. Kawaguchi, T. Yamashita, G.-i. Katahira, H. Yokozawa, T. Torigoe, N. Sato, *Spine* **2002**, *27*, 1511.
- [40] Y. Lu, Q. Xue, M. R. Eisele, E. S. Sulistijo, K. Brower, L. Han, E.-a. D. Amir, D. Pe'er, K. Miller-Jensen, R. Fan, *Proc. Natl. Acad. Sci. USA* **2015**, *112*, 607.
- [41] H. An, Y. Yu, M. Zhang, H. Xu, R. Qi, X. Yan, S. Liu, W. Wang, Z. Guo, J. Guo, *Immunology* **2002**, *106*, 38.
- [42] D. Y. Vogel, J. E. Glim, A. W. Stavenuiter, M. Breur, P. Heijnen, S. Amor, C. D. Dijkstra, R. H. Beelen, *Immunobiology* **2014**, *219*, 695.
- [43] S. Gordonov, M. K. Hwang, A. Wells, F. B. Gertler, D. A. Lauffenburger, M. Bathe, *Integr. Biol.* **2016**, *8*, 73.
- [44] A. Salah, A. Rane, L. Xiao, C. Honrado, X. Li, L. Jin, N. S. Swami, *Biosens. Bioelectron.* **2022**, *210*, 114346.
- [45] A. Jacobs, L. Ignarro, *J. Biol. Chem.* **2001**, *276*, 47950.
- [46] C. Petchakup, P. E. Hutchinson, H. M. Tay, S. Y. Leong, K. H. H. Li, H. W. Hou, *Sens. Actuators, B* **2021**, *339*, 129864.
- [47] D. W. Inglis, *Appl. Phys. Lett.* **2009**, *94*, 013510.
- [48] D. Di Carlo, D. Irimia, R. G. Tompkins, M. Toner, *Proc. Natl. Acad. Sci. USA* **2007**, *104*, 18892.
- [49] D. Di Carlo, *Lab Chip* **2009**, *9*, 3038.
- [50] D. Spencer, H. Morgan, *Lab Chip* **2011**, *11*, 1234.
- [51] V. Errico, A. De Ninno, F. R. Bertani, L. Businaro, P. Bisegna, F. Caselli, *Sens. Actuators, B* **2017**, *247*, 580.